J. Appl. Comput. Mech., 9(4) (2023) 955-973
DOI: 10.22055/jacm.2023.42530.3941

ISSN: 2383-4536
jacm.scu.ac.ir

Shahid Chamran University of Ahvaz

Journal of Applied and Computational Mechanics

Research Paper

Comparative Study of the Spectral Method, DISPERSE and Other Classical Methods for Plotting the Dispersion Curves in Anisotropic Plates

Ismaine Zitouni, Hassan Rhimini, Abdelkerim Chouaf

Laboratory of Mechanics, Engineering and Innovation, National High School of Electricity and Mechanics, Hassan II University, Casablanca, Morocco
Email: Ismaine.zitouni.doc20@ensem.ac.ma (I.Z.); h.rhimini@ensem.ac.ma (H.R.); a.chouaf@ensem.ac.ma (A.C.)

Received December 13 2022; Revised February 26 2023; Accepted for publication March 22 2023.
Corresponding author: I. Zitouni (Ismaine.zitouni.doc20@ensem.ac.ma)

Abstract. This paper presents a comparative study of different methods for obtaining the dispersion curves of ultrasonic guided waves in anisotropic media. First, we present the classical algorithms used to find zeros and propose some improvements. Next, the spectral method is explained for modeling the guided waves in anisotropic materials while presenting a technique that can distinguish the modes present in the structure. The dispersion curves are plotted using a Matlab program and the results are compared with those of the DISPERSE software. In addition, a comparison with the results obtained by Nayfeh's works in the field of Nondestructive testing by ultrasonic guided waves is included. Then a discussion is developed to highlight the strengths of the spectral method. For proper non-destructive testing, we need reliable information about the modes that propagate in our waveguide. Both analytical and spectral approaches have limitations in obtaining the exact displacement and stress profiles in a plate media. To remedy this, normalization by the acoustic power is essential. Next, the displacement and stress fields obtained from the spectral method of the modes that can propagate in the plate are compared to those obtained analytically. A very good concordance is then noticed. Based on the results obtained, the spectral method presents a very good alternative for obtaining dispersion curves. It is a convergent method, stable, easy to implement with a very low calculation time.

Keywords: Guided waves, anisotropic media, dispersion curves, spectral method, ultrasonic, normalized displacements.

1. Introduction

Ultrasonic Guided Waves (UGW) have been widely used in Non-Destructive Testing (NDT) of various structures. They are characterized by their ability to propagate over long distances while producing deformations through the entire thickness of the inspected piece. They, therefore, constitute a colossal way to control quickly and integrally pieces of large dimensions with difficult access areas without significant attenuation. However, these waves have a dispersive character making them very sensitive to frequency variation.

To control defects in structures by UGW, the first essential step is the knowledge of the dispersion curves. With these, the frequencies of the waves susceptible to propagate in the material have been determined. Thereafter, for the generation of these waves, a choice of the adequate frequency is essential. In the same way, several methods are used to draw these curves. In most cases, these methods are based on numerical simulations [1, 2], on data provided by experiments [3, 4], and also by the development of programs in Matlab based on roots finding algorithms of characteristic functions [5-7]. For solving the characteristic dispersion equations, we found in the literature researchers who use linear or quadratic iterative algorithms known to be fast in finding a single root [8, 9]. Unfortunately, when the characteristic function has more than one zero or two near roots, these methods face difficulties and become unstable. Other algorithms use slower but safer iteration techniques, such as the Newton-Raphson [5, 6] and Bisection [7] algorithms. However, a large number of operations, especially in multilayer and cylindrical structures, make these methods limited and slow [10]. Waas [11] introduced the Semi-Analytic Finite Element (SAFE) method for the study of the wave propagation in elastic and viscoelastic media with a planar and axisymmetric geometries. This allowed the analysis of vertical and torsional vibration of a multilayer soil. Ahmad et al. [12] applied the SAFE method for plotting the dispersion curves of an aluminum plate and a composite structure. Salah et al. [13] extended this method for the analysis of materials with orthorhombic symmetry. The SAFE method was justified by Barazanchy and Giurgiutiu [14] as a robust method by comparing it with Disperse software [15].

New method has been introduced for the modeling of the UGW, it is the spectral method (SM). Spectral schemas are often used to solve differential equations. But instead of a direct calculation, the researchers used a spectral approximation for the solution that satisfies the propagating differential equation and boundary conditions. So, the problem is reformulated as an eigenvalue problem. The derivation operators are then approximated by differentiation matrices with spectral precision, so the eigenvalue problem is formulated in a matrix form. Once the eigenvalue problem is solved, it provides both eigenvalue (frequency) and eigenvector (displacement) solutions. Even though this method has been successfully used to solve a large range of differential equations, it is still under development for obtaining dispersion curves of guided waves. Adamou [16] was among the first to introduce the spectral method for the determination of the UGW dispersion curves. He tested the robustness of the method by treating anisotropic, inhomogeneous and multilayer media. Karpfinger et al. [17-18] applied the SM to multilayer cylindrical structures of isotropic materials. They used the SM to solve the dispersion equations for the case of cylindrical poroelastic structures. Yu et al. [19] characterized by the SM the dispersion curves of longitudinal modes of multilayer isotropic cylindrical media. Quintanilla et al. [20-22] have plotted by the SM the dispersion curves of most complex waveguides. These waveguides can be summarized as perfectly elastic homogeneous anisotropic materials in planar, cylindrical and multilayer geometry. Another method based on the Legendre formalism [23] has been used by many researchers. It is based on a polynomial approach for solving the equation of motion [24, 25]. There are also methods based on Cauchy formalism [26]. Based on these curves we can perform finite element numerical simulations of structures to detect defects. Although many methods have been proposed to study the dispersive character of the UGW, more reliable and robust approaches are still needed. They will improve the accuracy and efficiency analysis of the complex propagation of these waves.

Our work presented here consists in realizing a comparative study of various methods for obtaining the dispersion curves, that is, the analytical classical methods, the spectral method and the DISPERSE software [15]. This study aims to provide a clear overview of the advantages and disadvantages of each method, it will make it easier for the user to choose between these methods. Our comparison takes into account the computation time, the convergence of these methods and the coding efforts of each algorithm. The mathematical formulations of each method are also presented in the following paragraphs. Moreover, the accuracy of the found solutions is proved by the comparison with the previous works of Nayfeh [27]. We chose this scholar because he was one of the first researchers to have worked on the plotting of dispersion curves analytically and also several references took him as a reference. The study is carried out for four types of materials: isotropic, transverse isotropic, orthotropic and monoclinic. In each symmetry, we have shown the most adequate method for plotting the dispersion curves.

To generate the UGW in our structure and make an adequate control, we need an adapted choice of the frequency (dispersion curves) as well as information on the generated mode (displacements and stresses). Similarly, the analytical profiles of displacements and stresses normalized by acoustic power are plotted through the thickness of the plates and are compared to the profiles of the eigenvectors obtained from the spectral method for different values of the couple frequency, wave number (f,k).

2. Guided Waves Theory in Plates

We considered a homogeneous anisotropic plate, unlimited in the x_1 and x_2 directions and with thickness $d = 2h$ along the x_3 axis (Fig. 1). We limited the study to cut specimens so that the $x_1^{'}$ and $x_2^{'}$ axes of the crystallographic reference are contained in the median plane and the $x_3^{'}$ axis is normal to the plate. We consider that the direction of propagation coincides with the x_1 axis. In the most general case, this propagation direction is not a principal direction, and the global Cartesian coordinate system (x_1,x_2,x_3) used to study propagation is derived from the reference Cartesian system $(x_1^{'},x_2^{'},x_3^{'})$ by the angular rotation ϕ around the x_3 axis (Fig. 1). The equations that govern the elastic waves in an anisotropic plate are written in the Cartesian reference system $x_i^{'}=(x_1^{'},x_2^{'},x_3^{'})$ as follows:

$$\frac{\partial \sigma_{ij}^{'}}{\partial x_i^{'}} = \rho^{'} \frac{\partial^2 u_i^{'}}{\partial t^2} \tag{1}$$

We remind that Hooke's law is given by:

$$\sigma_{ij}^{'} = c_{ijkl}^{'} \varepsilon_{kl}^{'} \tag{2}$$

and the deformation-displacement relationship is as follows:

$$\varepsilon_{kl}^{'} = \frac{1}{2}\left(\frac{\partial u_k^{'}}{\partial x_l^{'}} + \frac{\partial u_l^{'}}{\partial x_k^{'}}\right) \tag{3}$$

For the stress σ' and strain ε' symmetric tensors, we adopted the same notation of contracted indices mentioned before. As a result, Hooke's law is written in the following extended matrix form:

$$\begin{Bmatrix} \sigma_{11}^{'} \\ \sigma_{22}^{'} \\ \sigma_{33}^{'} \\ \sigma_{23}^{'} \\ \sigma_{13}^{'} \\ \sigma_{12}^{'} \end{Bmatrix} = \begin{bmatrix} c_{11}^{'} & c_{12}^{'} & c_{13}^{'} & c_{14}^{'} & c_{15}^{'} & c_{16}^{'} \\ & c_{22}^{'} & c_{23}^{'} & c_{24}^{'} & c_{25}^{'} & c_{26}^{'} \\ & & c_{33}^{'} & c_{34}^{'} & c_{35}^{'} & c_{36}^{'} \\ & & & c_{44}^{'} & c_{45}^{'} & c_{46}^{'} \\ & \text{sym} & & & c_{55}^{'} & c_{56}^{'} \\ & & & & & c_{66}^{'} \end{bmatrix} \begin{Bmatrix} \varepsilon_{11}^{'} \\ \varepsilon_{22}^{'} \\ \varepsilon_{33}^{'} \\ \varepsilon_{23}^{'} \\ \varepsilon_{13}^{'} \\ \varepsilon_{12}^{'} \end{Bmatrix} \tag{4}$$

The density of the material is a scalar and stays invariant before and after the change of the reference. Therefore, the elastic stiffness tensor in the local coordinate system $(x_1^{'},x_2^{'},x_3^{'})$ will be transformed into the global system (x_1,x_2,x_3) as follows:

$$C_{mnop} = \beta_{mi}\beta_{nj}\beta_{ok}\beta_{pl} c_{ijkl_{mn}}^{'} \tag{5}$$

where β_{ij} is the transformation tensor that contains the cosine of the angles between the x_i and $x_j^{'}$ axes in the general case. m, n, o, p = 1, 2, 3.

For the case of a rotation around the x_3 axis, the transformation is described by:

$$\beta_{ij} = \begin{bmatrix} \cos(\phi) & \sin(\phi) & 0 \\ -\sin(\phi) & \cos(\phi) & 0 \\ 0 & 0 & 1 \end{bmatrix} \tag{6}$$

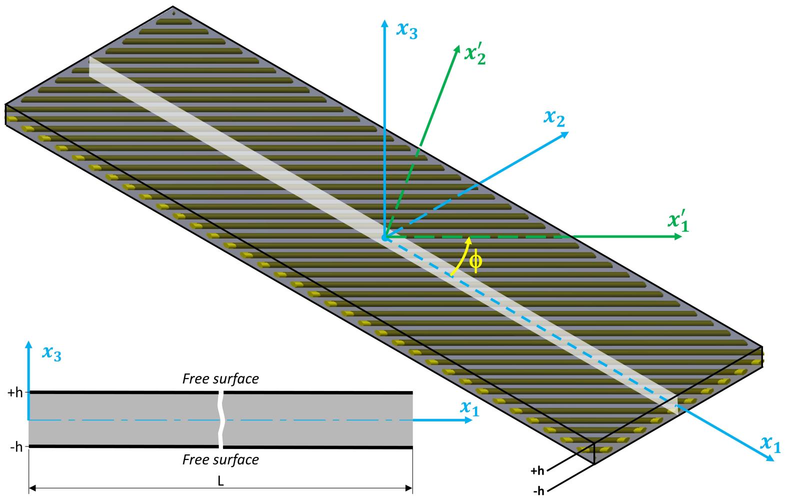

Fig. 1. Geometry of the plate, (x_1, x_2, x_3): Global Cartesian coordinate system. (x_1', x_2', x_3'): Cartesian reference system, x_1: propagation direction, grey rectangle: sagittal plane.

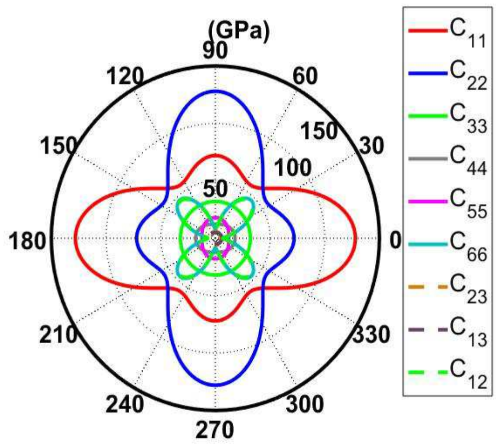

Fig. 2. Transformation stiffness tensor components versus ϕ of orthotropic plate.

Then the number of the non-null elasticity constant of the new tensor is larger, for example, for any ϕ angle, the representative tensor of an orthotropic material is transformed into a representative tensor of a fictive monoclinic material.

The equation of motion Eq. (1), Hooke's law and the deformation-displacement relationship are transformed into:

$$\frac{\partial \sigma_{ij}}{\partial x_i} = \rho \frac{\partial^2 u_i}{\partial t^2} \tag{7}$$

$$\sigma_{ij} = C_{ijkl}\varepsilon_{kl} \tag{8}$$

$$\varepsilon_{kl} = \frac{1}{2}\left(\frac{\partial u_k}{\partial x_l} + \frac{\partial u_l}{\partial x_k}\right) \tag{9}$$

In order to better assimilate the behavior of the elastic constants according to the rotation angle ϕ, we will consider in the following the example of a material with orthotropic symmetry.

Figure 2 shows the variation of the elastic constants of an orthotropic material (table 1) according to the ϕ angle. For angles of 0°, 90°, 180° and 270° the constants C_{16}, C_{26}, C_{36} and C_{45} are null and the orthotropic material will be described by these nine constants: C_{11}, C_{22}, C_{33}, C_{44}, C_{55}, C_{66}, C_{12}, C_{13} and C_{23}, on the other hand for angles different from those mentioned before, the constants C_{16}, C_{26}, C_{36} and C_{45} have non-zero values.

Table 1. Elastic stiffness tensor components of an orthotropic plate; c'_{ij} (GPa) and ρ (10^3 kg/m^3).

c'_{11}	c'_{12}	c'_{13}	c'_{22}	c'_{23}	c'_{33}	c'_{44}	c'_{55}	c'_{66}	ρ
128	7	6	72	5	32	18	12.5	8	2

To study the nature of the different guided modes that are susceptible to propagate in the plates, we consider an infinite anisotropic plate with triclinic symmetry. In this media, we see that symmetrical (S_n) and antisymmetrical (A_n) modes of vibration appear, which we call Lamb modes, and which are most commonly coupled to horizontally shear modes (SH_n).

The general form of the solution is:

$$u_j = U_j e^{ik(x_1+\alpha x_3-ct)} \tag{10}$$

With *k* is the wave number along the x_1 direction, α is the ratio of the wave numbers along the x_1 and x_3 directions, *c* is the phase velocity, and i (non-italic) is the imaginary unit ($i^2 = -1$).

The equation of motion can be written also as follows:

$$C_{ijkl}u_{k,jl} = \rho \ddot{u}_i \tag{11}$$

where C_{ijkl} is the tensor of the elastic constants, $u_{k,jl}$ is the second derivative of the displacement vector, ρ is the density, and $\ddot{u}_i$ represents the acceleration vector.

Substituting Eq. (10) into Eq. (11), we obtain the matrix form of the Christoffel equations:

$$K_{mn}(\alpha)U = 0 \tag{12}$$

where *m*, *n* = 1, 2, 3. The expressions of the elements of the matrix *K* [27] are:

$$\begin{cases} K_{11} = C_{11} - \rho c^2 + 2C_{15}\alpha + C_{55}\alpha^2 \\ K_{12} = C_{16} + (C_{14} + C_{56})\alpha + C_{45}\alpha^2 \\ K_{13} = C_{15} + (C_{13} + C_{55})\alpha + C_{35}\alpha^2 \\ K_{22} = C_{66} - \rho c^2 + 2C_{46}\alpha + C_{44}\alpha^2 \\ K_{23} = C_{56} + (C_{36} + C_{45})\alpha + C_{34}\alpha^2 \\ K_{33} = C_{55} - \rho c^2 + 2C_{35}\alpha + C_{33}\alpha^2 \end{cases} \tag{13}$$

We have adopted the following contracted index notation: 1→ 11, 2→ 22, 3→ 33, 4→ 23, 5→ 13 and 6→ 12.

U is the vector of amplitudes of displacements and C_{ij} are the components of stiffness. The existence of nontrivial solutions for *U* requires the annulation of the determinant of *K*, which is a sixth-degree polynomial equation in α. For any value of *c*, there are therefore six distinct solutions α_q.

Considering the K_{mn} terms expressed in Eq. (13), we calculate the following ratios V_q and W_q:

$$\begin{cases} V_q = \dfrac{U_{2q}}{U_{1q}} = \dfrac{K_{11}(\alpha_q)K_{23}(\alpha_q) - K_{13}(\alpha_q)K_{12}(\alpha_q)}{K_{13}(\alpha_q)K_{22}(\alpha_q) - K_{12}(\alpha_q)K_{23}(\alpha_q)} \\ W_q = \dfrac{U_{3q}}{U_{1q}} = \dfrac{K_{11}(\alpha_q)K_{23}(\alpha_q) - K_{13}(\alpha_q)K_{12}(\alpha_q)}{K_{12}(\alpha_q)K_{33}(\alpha_q) - K_{23}(\alpha_q)K_{13}(\alpha_q)} \end{cases} \tag{14}$$

The expressions of the stresses σ_{33}, σ_{13} and σ_{23} are obtained using those of V_q and W_q defined earlier and the Hooke's law:

$$(\sigma_{33}, \sigma_{13}, \sigma_{23}) = \sum_{q=1}^{6} ik(D_{1q}, D_{2q}, D_{3q})U_{1q}e^{ik(x_1+\alpha x_3-ct)} \tag{15}$$

where the expressions of the stress amplitudes are given by:

$$\begin{cases} D_{1q} = C_{13} + \alpha_q C_{35} + (C_{36} + \alpha_q C_{34})V_q + (C_{35} + \alpha_q C_{33})W_q \\ D_{2q} = C_{15} + \alpha_q C_{55} + (C_{56} + \alpha_q C_{45})V_q + (C_{55} + \alpha_q C_{35})W_q \\ D_{3q} = C_{14} + \alpha_q C_{45} + (C_{46} + \alpha_q C_{44})V_q + (C_{45} + \alpha_q C_{34})W_q \end{cases} \tag{16}$$

Therefore, we can write the boundary conditions for the free plate, that is, the cancellation of the stresses σ_{33}, σ_{13} and σ_{23} at the top and bottom surfaces $(x_3 = \pm h)$, which give a system of 6 equations on the amplitudes U_{11} ..., U_{16}. The existence of non-trivial solutions requires the annulation of the determinant.

At this stage, several algorithms for finding zeros have been used [5-7]. In the following paragraphs, we will review the principles of roots finding methods of characteristic functions and propose refinements to improve their speed and efficiency.

3. Roots Finding Algorithms Methods

3.1 Bisection method

The bisection method or dichotomy method [7, 28] belongs to the family of bracketing methods. It has the advantage of being robust, its algorithm is theoretically convergent and easy to program. The principle of this method is the searching for the zero of a continuous function on an interval in which the function changes the sign at its limits. In our case, we seek to determine the couple's frequency, wave number (f, k) that allow the cancellation of the guided wave characteristic functions for a range of frequency and wave number. This range as well as the wave number and frequency steps for which the dispersion curves should be obtained are fixed. The general procedure is then to fix the first wave number step and to evaluate the characteristic function at each frequency step. A scan of the entire frequency range is then performed. Modal solutions are found wherever the characteristic functions change signs between two frequency steps.

It should be noted that the dispersion equation shows a discontinuity, especially in the neighborhood of real roots. To avoid solutions resulting from these discontinuities, we check whether the absolute value of the characteristic function is a minimum (Fig. 3).

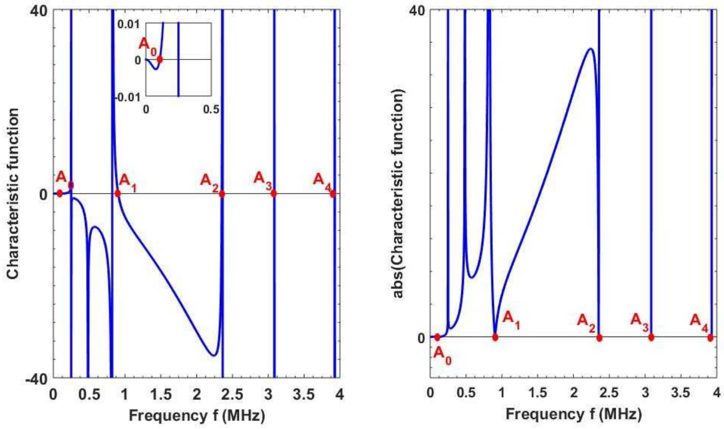

Fig. 3. (a) Evaluation of the characteristic function for antisymmetric modes at a wave number k = 500 m^{-1} in 2 mm thickness of an aluminum alloy plate. (b) The minima in the absolute value mark the modal solution.

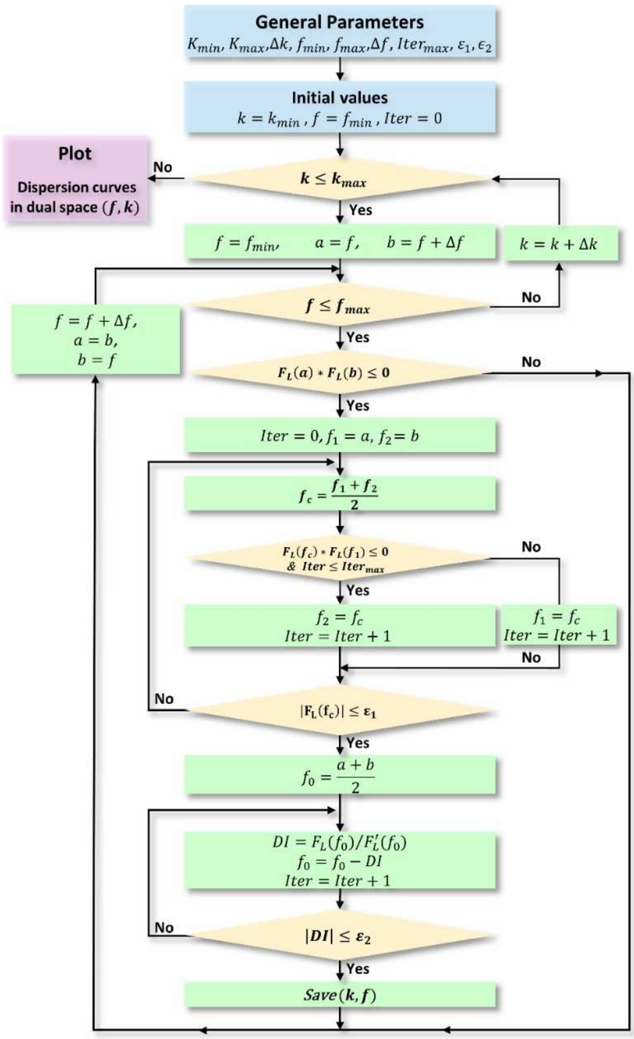

Fig. 4. Hybrid flowchart for plotting dispersion curves.

This procedure is repeated for each step of k until the desired final value of the wave number k is attained. The dispersion curves are then found and plotted in the dual plane (fd, k). Other forms of the dispersion curves can be deduced from the expressions that relate the frequency, the wave number to other quantities such as the phase velocity and the group velocity. This procedure provides satisfying results for isotropic plates, but it is still very slow or even inadequate when the material is anisotropic or when the structure is composed of several layers.

3.2 Newton method

Newton's method, also called the Newton-Raphson method, is among the most famous algorithms for finding zeros [29]. It is distinguished by the fact that both the function and its derivative must be evaluated at arbitrary points. It has been the subject of several research works to determine the dispersion curves [5, 6]. In the same way as the bisection method, we have evaluated in our case the characteristic function along the frequency interval at each wave number step. Therefore, this time instead of discretizing the frequency domain into steps of frequencies at each iteration, we used the tangent to the curve to approximate the solution. A procedure has been developed to eliminate the roots coming from discontinuity by checking the minima. Moreover, precautions have been taken to avoid iterations in infinite loops or when the zero searched is outside the frequency domain. Since Newton's method converges quadratically, the roots were obtained very quickly. However, in some places, the roots were close to each other, which made it difficult to confirm the uniticity of the solution. A jump of the solution is then considered, and will be subsequently recalculated by interpolation of the two solutions that frame it.

The choice of wave number steps Δk and frequency Δf was very important to have accurate dispersion curves. Despite the fast convergence of the method, it can converge to zeros that are not true modes. The initial values of (k, f_0) must be close to the zeros of the characteristic function. Therefore, it was difficult to satisfy this condition due to the complexity of the characteristic functions.

3.3 Hybrid method

Several researchers have proved that traditional root-finding algorithms are slow and require a fastidious computational time [10, 11]. They may have several limitations, especially when two zeros are very close, which may result in one or both of them being missed. In addition, these methods have been computationally intensive, have a large number of iterations, and can be difficult to implement especially when the material presents an anisotropy behavior or when the structure is formed of multilayered media.

In this section, we have proposed a hybrid algorithm that benefits from the certitude of convergence presented by the bisection method and the speed of convergence proper to the Newton method. For this purpose, we first started the search for zeros by the bisection method for a break test ε_1. The value of f_0 was approximated by the bisection method, subsequently, we used Newton's method for a second break test ε_2 in which $\varepsilon_1 > \varepsilon_2$ (Fig. 4).

The only relevant problem that this method may have, which largely comes back to the theory of Newton's method, is the ignorance of the derivative of the characteristic function. This derivative is calculated numerically, but it affects the speed of convergence.

4. Spectral Method

4.1 Basic formulation

The analysis will be conducted in the global Cartesian system, in which the ultrasonic guided wave propagates on the sagittal plane in the x_1 direction and retains its independence properties with respect to the x_2 coordinate $(\partial / \partial x_2 = 0)$. Therefore, the displacements that satisfy the propagation equation Eq. (11) have components of the form:

$$u = \begin{Bmatrix} u_1 \\ u_2 \\ u_3 \end{Bmatrix} = \begin{Bmatrix} U_1(x_3) \\ U_2(x_3) \\ U_3(x_3) \end{Bmatrix} e^{i(kx_1 - \omega t)} \tag{17}$$

where ω is the angular frequency

The expressions of the stresses are then written in the form:

$$\begin{cases} \sigma_{11} = [ikC_{11} + C_{15}\frac{\partial}{\partial x_3}]u_1 + [ikC_{16} + C_{14}\frac{\partial}{\partial x_3}]u_2 + [ikC_{15} + C_{13}\frac{\partial}{\partial x_3}]u_3 \\ \sigma_{22} = [ikC_{12} + C_{25}\frac{\partial}{\partial x_3}]u_1 + [ikC_{26} + C_{24}\frac{\partial}{\partial x_3}]u_2 + [ikC_{25} + C_{23}\frac{\partial}{\partial x_3}]u_3 \\ \sigma_{33} = [ikC_{13} + C_{35}\frac{\partial}{\partial x_3}]u_1 + [ikC_{36} + C_{34}\frac{\partial}{\partial x_3}]u_2 + [ikC_{35} + C_{33}\frac{\partial}{\partial x_3}]u_3 \\ \sigma_{23} = [ikC_{14} + C_{45}\frac{\partial}{\partial x_3}]u_1 + [ikC_{46} + C_{44}\frac{\partial}{\partial x_3}]u_2 + [ikC_{45} + C_{34}\frac{\partial}{\partial x_3}]u_3 \\ \sigma_{13} = [ikC_{15} + C_{55}\frac{\partial}{\partial x_3}]u_1 + [ikC_{56} + C_{45}\frac{\partial}{\partial x_3}]u_2 + [ikC_{55} + C_{35}\frac{\partial}{\partial x_3}]u_3 \\ \sigma_{12} = [ikC_{16} + C_{56}\frac{\partial}{\partial x_3}]u_1 + [ikC_{66} + C_{46}\frac{\partial}{\partial x_3}]u_2 + [ikC_{56} + C_{36}\frac{\partial}{\partial x_3}]u_3 \end{cases} \tag{18}$$

The propagation equation Eq. (11) can be written in the following form:

$$\begin{cases} [-k^2C_{11} + 2ikC_{15}\frac{\partial}{\partial x_3} + C_{55}\frac{\partial^2}{\partial x_3^2}]U_1 + [-k^2C_{16} + ik(C_{14} + C_{56})\frac{\partial}{\partial x_3} + C_{45}\frac{\partial^2}{\partial x_3^2}]U_2 + [-k^2C_{15} + ik(C_{13} + C_{55})\frac{\partial}{\partial x_3} + C_{35}\frac{\partial^2}{\partial x_3^2}]U_3 = -\rho\omega^2 U_1 \\ [-k^2C_{16} + ik(C_{14} + C_{56})\frac{\partial}{\partial x_3} + C_{45}\frac{\partial^2}{\partial x_3^2}]U_1 + [-k^2C_{66} + 2ikC_{46}\frac{\partial}{\partial x_3} + C_{44}\frac{\partial^2}{\partial x_3^2}]U_2 + [-k^2C_{56} + ik(C_{36} + C_{45})\frac{\partial}{\partial x_3} + C_{34}\frac{\partial^2}{\partial x_3^2}]U_3 = -\rho\omega^2 U_2 \\ [-k^2C_{15} + ik(C_{13} + C_{55})\frac{\partial}{\partial x_3} + C_{35}\frac{\partial^2}{\partial x_3^2}]U_1 + [-k^2C_{56} + ik(C_{36} + C_{45})\frac{\partial}{\partial x_3} + C_{35}\frac{\partial^2}{\partial x_3^2}]U_2 + [-k^2C_{55} + 2ikC_{35}\frac{\partial}{\partial x_3} + C_{33}\frac{\partial^2}{\partial x_3^2}]U_3 = -\rho\omega^2 U_3 \end{cases} \tag{19}$$

The problem can be rewritten as an eigenvalue problem:

$$\begin{bmatrix} A & B & C \\ D & E & F \\ G & H & K \end{bmatrix}_{(3,3)} \begin{Bmatrix} U_1 \\ U_2 \\ U_3 \end{Bmatrix}_{(3,1)} = \omega^2 \begin{bmatrix} -\rho & 0 & 0 \\ 0 & -\rho & 0 \\ 0 & 0 & -\rho \end{bmatrix}_{(3,3)} \begin{Bmatrix} U_1 \\ U_2 \\ U_3 \end{Bmatrix}_{(3,1)} \tag{20}$$

With the expressions of the different components of the matrix:

$$\begin{cases} A = -k^2C_{11} + 2ikC_{15}\dfrac{\partial}{\partial x_3} + C_{55}\dfrac{\partial^2}{\partial x_3^2} \\ B = -k^2C_{16} + ik(C_{14} + C_{56})\dfrac{\partial}{\partial x_3} + C_{45}\dfrac{\partial^2}{\partial x_3^2} \\ C = -k^2C_{15} + ik(C_{13} + C_{55})\dfrac{\partial}{\partial x_3} + C_{35}\dfrac{\partial^2}{\partial x_3^2} \\ D = -k^2C_{16} + ik(C_{14} + C_{56})\dfrac{\partial}{\partial x_3} + C_{45}\dfrac{\partial^2}{\partial x_3^2} \\ E = -k^2C_{66} + 2ikC_{46}\dfrac{\partial}{\partial x_3} + C_{44}\dfrac{\partial^2}{\partial x_3^2} \\ F = -k^2C_{56} + ik(C_{36} + C_{45})\dfrac{\partial}{\partial x_3} + C_{34}\dfrac{\partial^2}{\partial x_3^2} \\ G = -k^2C_{15} + ik(C_{13} + C_{55})\dfrac{\partial}{\partial x_3} + C_{35}\dfrac{\partial^2}{\partial x_3^2} \\ H = -k^2C_{56} + ik(C_{36} + C_{45})\dfrac{\partial}{\partial x_3} + C_{35}\dfrac{\partial^2}{\partial x_3^2} \\ K = -k^2C_{55} + 2ikC_{35}\dfrac{\partial}{\partial x_3} + C_{33}\dfrac{\partial^2}{\partial x_3^2} \end{cases} \tag{21}$$

The boundary conditions for a stressed free-face plate are expressed as:

$$\begin{cases} \sigma_{33}(\pm h) = 0 \\ \sigma_{23}(\pm h) = 0 \\ \sigma_{13}(\pm h) = 0 \end{cases} \tag{22}$$

In matrix notation, the boundary conditions are written:

$$\begin{bmatrix} BC_1 & BC_2 & BC_3 \\ BC_4 & BC_5 & BC_6 \\ BC_7 & BC_8 & BC_9 \end{bmatrix}_{(3,3)} \begin{Bmatrix} U_1(\pm h) \\ U_2(\pm h) \\ U_3(\pm h) \end{Bmatrix}_{(3,1)} = \begin{Bmatrix} 0 \\ 0 \\ 0 \end{Bmatrix}_{(3,1)} \tag{23}$$

with the expression of the BC_i components:

$$\begin{cases} BC_1 = ikC_{14} + C_{45}\dfrac{\partial}{\partial x_3} \\ BC_2 = ikC_{46} + C_{44}\dfrac{\partial}{\partial x_3} \\ BC_3 = ikC_{45} + C_{34}\dfrac{\partial}{\partial x_3} \\ BC_4 = ikC_{15} + C_{55}\dfrac{\partial}{\partial x_3} \\ BC_5 = ikC_{56} + C_{45}\dfrac{\partial}{\partial x_3} \\ BC_6 = ikC_{55} + C_{35}\dfrac{\partial}{\partial x_3} \\ BC_7 = ikC_{13} + C_{35}\dfrac{\partial}{\partial x_3} \\ BC_8 = ikC_{36} + C_{34}\dfrac{\partial}{\partial x_3} \\ BC_9 = ikC_{35} + C_{33}\dfrac{\partial}{\partial x_3} \end{cases} \tag{24}$$

Now our matrix system is defined by three equations of motion and six equations for the boundary conditions. We will try to solve the eigenvalue problem by the spectral method, for this purpose in the first step we will replace the differential operators defined in x_3 by Chebyshev differentiation matrices (DM) based on a nonuniform distribution of N points for a bounded interval. With the Matlab function chebdif [30], this step has become easier and we resume it in Fig. 5.

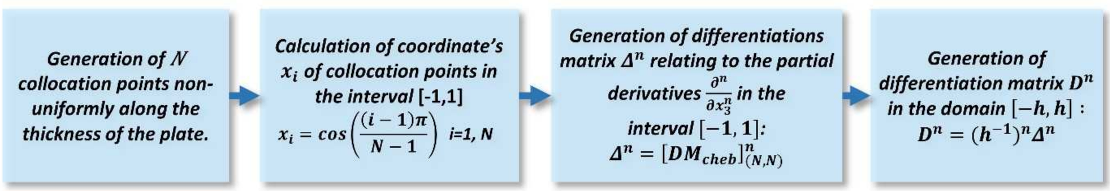

Fig. 5. Block diagram of the Chebyshev method.

The second step consists in obtaining our solutions using the *eig* procedure of Matlab dedicated to solve eigenvalue and eigenvector problems. We replaced the partial derivatives in x_3 by the differentiation matrices generated by the Chebyshev approximation and we obtained the different expressions of the components of the matrices defined in Eq. (21) and Eq. (24). Note that when replacing the derivatives by the differentiation matrices, we have to multiply the terms without derivatives by the identity matrix $I_{(N,N)}$ to avoid the problem of sizing of matrices.

We note that in the displacement vector, the lines from 1 to *N* correspond to U_1, from N+1 to 2*N* correspond to U_2 and from 2*N*+1 to 3*N* correspond to U_3. The boundary conditions at $x_3 = \pm h$ are therefore respectively 1 and *N* for U_1, *N*+1 and 2*N* for U_2 and 2*N*+1 and 3*N* for U_3.

4.2 Mode separation

In anisotropic materials with the propagation direction along any ϕ angle, the horizontally shear (SH) modes are coupled to the symmetrical and antisymmetrical Lamb modes. While isotropic, orthotropic, or transverse isotropic materials with ϕ angles of 0° and 90°, the SH modes are uncoupled from the Lamb modes [31].

When plotting the dispersion curves, whatever the algorithm used, we noticed that when the modes are close, there is always a crossing of modes. This phenomenon occurs especially when symmetric, antisymmetric and SH modes are coupled. In order to differentiate between these modes, Quintanilla [22] proposed two criteria based on the parity and the decoupling of the Christoffel equations. Both criteria are tested on several examples. The modes are separated and are well distinguished.

We have developed an efficient procedure to classify the obtained results by exploiting the symmetry and antisymmetry properties of Lamb and SH modes.

Pure Lamb modes are characterized by the nullity of the u_2 displacement component on either side of the plate thickness $(u_2(+h) = u_2(-h) = 0)$, to separate between symmetrical and antisymmetrical modes, you just have to check the symmetry of the displacements.

The SH waves are polarized along the x_2 direction horizontally, so they are characterized by the nullity of the component's displacement u_1 and u_3 through the plate thickness $(u_1(+h) = u_1(-h) = u_3(+h) = u_3(-h) = 0)$. Similarly, we have identified the two types of symmetric and antisymmetric SH waves. In the same way, we separate symmetric and antisymmetric modes using the symmetry of the u_2 displacement.

For materials with crystallographic symmetries of higher order (monoclinic), the SH modes are coupled to the Lamb modes. It is therefore difficult to separate them. The modes that propagate in the plate are the generalized Lamb modes. These modes are divided into two categories: symmetric and antisymmetric. The symmetrical modes have equal displacement components u_1 and u_2 on both sides of the plate $(u_1(+h) \times u_1(-h) > 0, u_2(+h) \times u_2(-h) > 0)$, and the u_3 components are opposite $(u_3(+h) \times u_3(-h) < 0)$. Concerning the antisymmetric modes, they present an opposite behavior.

4.3 Plotting the dispersion curves

We have developed a Matlab program to plot the dispersion curves in the plane (frequency-thickness, wave number) no matter the order of anisotropy of the material. The other representations: phase velocity V_p and group velocity V_g as a function of the frequency are deduced from the frequency and the wave number *k* via the following expressions:

$$\begin{cases} V_p = \dfrac{\omega}{k} \\ V_g = \dfrac{\partial \omega}{\partial k} \end{cases} \tag{25}$$

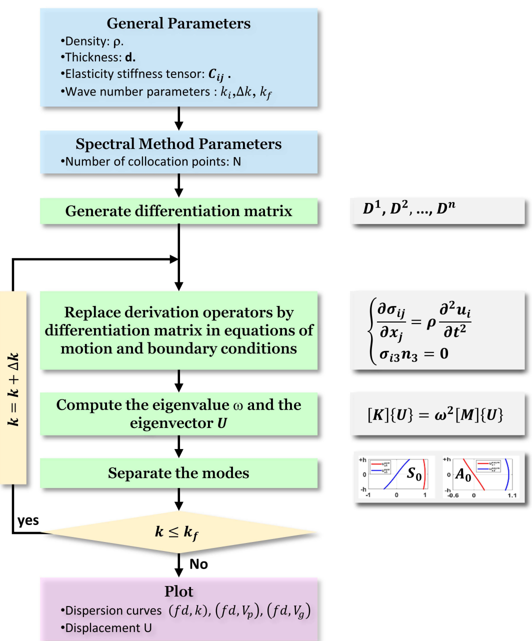

Fig. 6. Flowchart of the spectral method for plotting dispersion curves.

The flowchart in Fig. 6 explains the steps followed for plotting the dispersion curves. The first step is to define the mechanical parameters of the material and geometry of the plate: C_{ij}, ρ and d, as well as the size of the differentiation matrices and the number of collocation points. The second step is to replace the partial derivatives present in the equations of motion and boundary conditions with the differentiation matrices. For this purpose, a generation of N collocation points through the thickness is implemented. After the substitution of the partial derivatives by the differentiation matrices, the next step is the calculation of the eigenvalues and eigenvectors for each value of the wave number k. A classification based on the symmetric and antisymmetric properties of the modes is established. The final step is the plotting of the dispersion curves and the displacement profiles.

5. Disperse Software

Members of the Non-Destructive Testing Laboratory at Imperial College have developed a general use software package called DISPERSE that plot dispersion curves for a large range of structures. Subsequently, it allows to communicate the information contained in these curves efficiently. This software is based on the Global Matrix Method (GMM) which assembles both displacements and boundary conditions of all layers into a single global matrix (this is used to overcome the instabilities found by the Transfer Matrix Method developed in 1950). Isotropic and viscoelastic materials are fully supported, anisotropic materials are also covered, but are currently limited to the elastic plane case [15]. Once the dispersion curves are generated, DISPERSE provides many easy methods to explore and exploit the information from the curves. Among this information are the stress, displacements and energy distribution. Phase velocity, group velocity, attenuation, real wave number, incidence angle, can be visualized and used.

To validate our results, we have chosen to compare them with those from this software. We remind that this software is based on analytical equations and has obtained satisfaction from many researchers [13, 32-35].

6. Dispersion Curves

6.1 Isotropic material

For the first application, we were interested in the case of an isotropic aluminum plate with thickness d = 2 mm, Young's modulus E = 70 GPa, Poisson's ratio ν = 0.32 and mass density ρ = 2.7 g/cm^3. The plotted curves are from the bisection met hod (Fig. 7), Newton's method (Fig. 8a), hybrid method (Fig. 8b) and spectral method (Fig. 9).

In Fig. 7a, we have plotted the dispersion curves in the plane (frequency-thickness product, wave number) for the first 8 modes. These curves are obtained via a Matlab program based on the algorithms of the analytical methods (bisection, Newton and hybrid). The frequency step is chosen equal to 50 Hz and the final frequency is 6 MHz, that is fd = 12 MHz.mm. For the wave number, we used a step of 100 m^{-1} and a final value of 120000 m^{-1}. To obtain good dispersion curves (especially for small values of k), we performed our calculations in the (fd, k) plane and then converted them to the (fd, V_p) plane (Fig. 7b).

We observe that the curves obtained by the bisection method are in very good accordance with those obtained by the DISPERSE software. Except for very low wave number values, the DISPERSE software could not determine the roots of the Lamb characteristic equations (Fig. 7a).

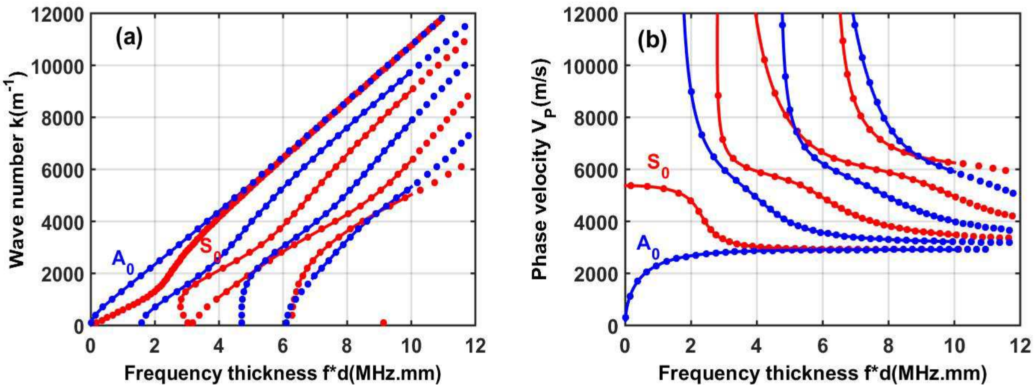

Fig. 7. Dispersion curves plotted by the bisection method (dotted lines) compared with those obtained by the DISPERSE software (solid lines) in the (fd, k) plane (a) and the (fd, V_p) plane (b).

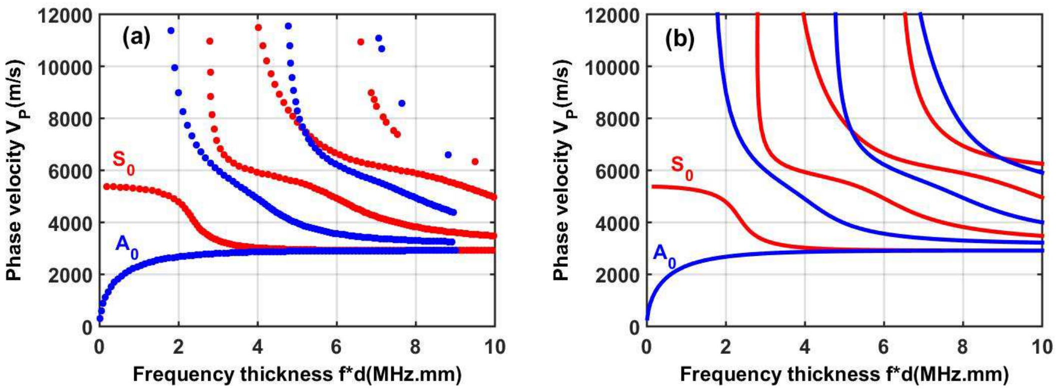

Fig. 8. (a) Dispersion curves plotted by the Newton method, (b) dispersion curves plotted by the hybrid method.

Table 2. Root square error for different values of the wave number k; RSE = √(fdBisection-fdNewton)².

k	S_0	S_1	A_0	A_1
100	1.6195 10^{-7}	1.9609 10^{-7}	2.8089 10^{-7}	3.5552 10^{-7}
300	3.8967 10^{-8}	1.4945 10^{-7}	2.2936 10^{-7}	2.7764 10^{-7}
500	1.6147 10^{-8}	1.6204 10^{-8}	3.5166 10^{-7}	1.9321 10^{-7}
1000	1.8611 10^{-7}	2.9624 10^{-7}	3.7147 10^{-7}	1.6189 10^{-7}

Table 3. Root square error for different values of the wave number k; RSE = √(fdBisection-fdHybrid)².

k	S_0	S_1	A_0	A_1
100	1.6197 10^{-7}	1.9607 10^{-7}	2.8089 10^{-7}	3.5545 10^{-7}
300	3.8960 10^{-8}	1.4945 10^{-7}	2.2936 10^{-7}	2.7765 10^{-7}
500	1.6147 10^{-8}	1.6204 10^{-8}	3.5166 10^{-7}	1.9321 10^{-7}
1000	1.8611 10^{-7}	2.9624 10^{-7}	3.7147 10^{-7}	1.6189 10^{-7}

Table 4. Root square error for different values of the wave number k; RSE = √(fdBisection-fdNewton)².

k	S_0	S_1	A_0	A_1
100	1.6184 10^{-7}	1.9609 10^{-7}	2.8137 10^{-7}	3.5551 10^{-7}
300	3.8981 10^{-8}	1.4946 10^{-7}	2.2935 10^{-7}	2.7764 10^{-7}
500	1.6155 10^{-8}	1.6202 10^{-8}	3.5466 10^{-7}	1.9324 10^{-7}
1000	1.8610 10^{-7}	2.9625 10^{-7}	3.7146 10^{-7}	1.6188 10^{-7}

Table 5. Comparison between the different methods used.

Method	Bisection	Newton	Hybrid	Spectral
Computing time (s)	870	627	588	0.6647
Number of iterations	6188	16843	11100	1 for each value of the wave number
Number of loops required	4	3	5	1
Treatment of the results	No	Yes	No	No

The dispersion curves obtained by the Newton algorithm in Fig. 8a showed some weaknesses, for example the S_3 and A_3 modes were not obtained completely. Moreover, the algorithm generates undesired solutions (solutions less than a product fd < 0). This problem has already been raised by some researchers in the case of the dispersion curve [6, 10].

All these problems are caused by the bad approximation of the initial value of the frequency f_0 which made the algorithm sometimes tend towards already found solutions or undesired solutions. A treatment of the results is necessary, which consists in eliminating all the negative roots found (because physically a frequency is never negative) as well as eliminating the roots already determined.

To overcome this problem and based on the results obtained previously, we proposed the hybrid method whose dispersion curves are presented in Fig. 8b. To test the convergence of these algorithms, we have presented the Tables 2 and 3 below which resume the RSE (Root Square Error) between the roots obtained by the bisection method and those obtained by the Newton and hybrid methods respectively of the first four modes.

The hybrid method benefited from the stability of the bisection method and the speed of convergence of the Newton method. The values obtained showed a very good concordance between the different methods for the plotting of the dispersion curves.

In Fig. 9, we presented the dispersion curves of the aluminum plate obtained by the spectral method using the number of collocation points N = 10. These were able to generate the first 16 modes defined in the whole range of the wave number. The quality of the dispersion curves obtained by the developed approach is approved by calculating the RSE presented in Table 4. This error is measured for the first four Lamb modes.

In this section, we have presented the results of several methods for plotting the dispersion curves. In order to see which of these methods proves to be the most efficient. In Table 5, a comparison based on different selected criteria has been established.

To obtain the results mentioned in Table 5, we used an *Intel(R) Core(TM) i5-5200U CPU @2.20GHz with 4G of RAM*.

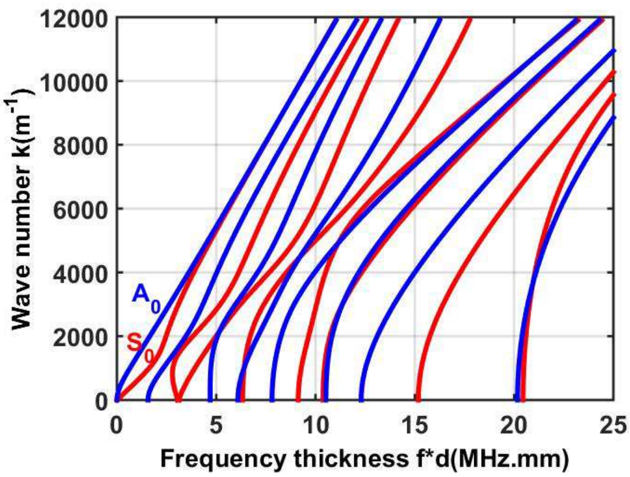

Fig. 9. Dispersion curves plotted by the spectral method.

Table 6. Elastic constants of a transverse isotropic plate (graphite-epoxy); c'_{ij} (GPa) and ρ (10^3 kg/m^3).

c'_{11}	c'_{12}	c'_{13}	c'_{22}	c'_{23}	c'_{33}	c'_{44}	c'_{55}	c'_{66}	ρ
155.6	3.7	3.7	15.95	4.33	15.95	5.81	7.46	7.46	1.6

Based on the results obtained above, the spectral method presented a very good alternative for obtaining the dispersion curves. It is a convergent method, easy to implement with very low computational time and stability. The convergence is obtained from values of N that obey the condition $(N \geq 2\pi / k)$ presented by Adamou [16]. The gain in computation time provided by the spectral method is not offered by other numerical methods such as SAFE method. Therefore, the robustness of this method in an anisotropic environment will be tested in the following.

In the following, we will treat the anisotropic behavior of materials. In this regard, different types of symmetries will be taken into account and the obtained solutions will be compared to those of the DISPERSE software.

6.2 Transverse isotropic material

We consider a transverse isotropic graphite-epoxy material, presenting a symmetry with invariance of the elastic constants around an axis of rotation, which reduces the independent number of elastic constants to 5. This class of material is widely used in multilayer structures [36]. The mass density and the stiffness matrix components considered are given in Table 6.

Figure 10a shows the dispersion curves of a graphite-epoxy composite plate obtained by the spectral method with the number of collocation points of N = 20. With these points, we quickly obtained the first 56 modes. In the first jet of these curves, we noticed that it was difficult to differentiate between the symmetrical, antisymmetrical and the SH modes. Moreover, when there is a mode crossing [37, 38] (area marked by a circle in Fig. 10a), we observed that for example, a symmetric mode before the overlap point becomes an antisymmetric mode which is wrong and will lead to problems in practice. In Fig. 10b we presented a zoom marked by the black ellipse of a mode crossing area situated at fd ≈ 1.5 MHz.mm (Fig. 10a). We considered four points A, B, C and D. A and C are taken before the crossing while B and D are taken after the crossing. The profiles of the displacements u_1 and u_3 of these four points are shown in Fig. 10b. If we take for example the path AB, we notice that the component u_1 passes from a symmetrical aspect to an antisymmetrical one and the same thing for the component u_3 which is false. The same remark was made for the path CD. The two curves must then take respectively the paths AD and CB. To overcome these problems, we used the mode separation, such that if the longitudinal and transverse displacement components are respectively on either side of the plate thickness equal and opposite then it is a symmetric Lamb mode. And if the longitudinal and transverse displacement components are respectively on either side of the plate thickness opposite and equal then it is an antisymmetric Lamb mode. For the SH modes, the same reasoning is applied but, now on the displacement u_2, a symmetrical horizontally shear mode has the displacements u_2 on both sides of the plate thickness equal. For antisymmetric modes, it is the opposite.

In Fig. 10c we presented the dispersion curves of Lamb modes with the separate symmetric and antisymmetric modes. Fig. 10d showed the dispersion curves of the SH modes with the separated symmetric and antisymmetric modes. With this technique, we were able to separate the Lamb modes from the SH modes since they are not coupled in the case of an orthotropic material with ϕ = 0° moreover the problem of mode changing due to mode crossing was no longer present.

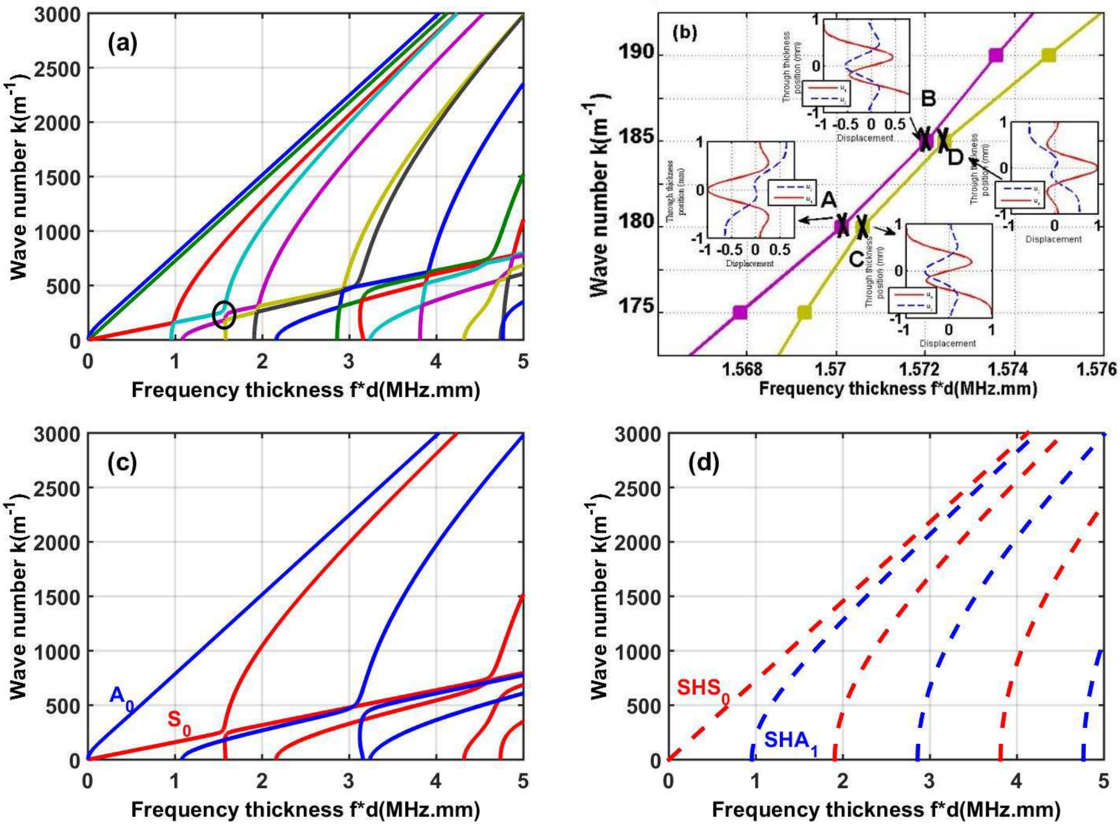

Fig. 10. Dispersion curves plotted by the spectral method without mode separation (a) and with mode separation (c-d) and a zoom on the first overlap in fd = 1.5 MHz.mm (b).

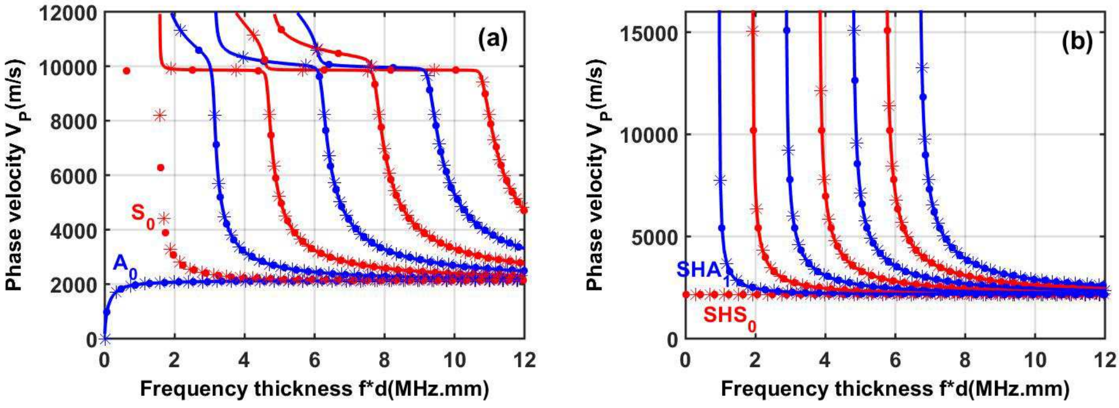

Fig. 11. (a and b) Dispersion curves for a graphite-epoxy composite plate of 4mm thickness and ϕ = 0°, plotted by: bisection method (•), DISPERSE software (continuous line) and the spectral method (star).

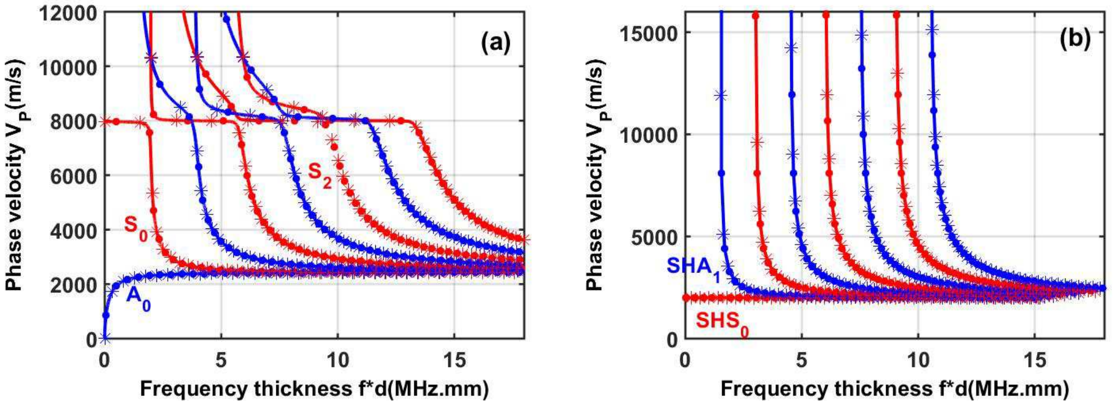

Fig. 12. (a and b) Dispersion curves for an orthotropic plate of 4mm thickness and ϕ = 0°, plotted by: bisection method (•), DISPERSE software (continuous line) and the spectral method (star).

We could see from Fig. 11 (a and b) that all three methods were able to plot the dispersion curves (Lamb modes and SH modes). Moreover, the curves are superposed on each other which reflects a very good convergence with an order error of 10^{-7}. However, the DISPERSE software encountered difficulties in plotting some modes such as the S_1 and SHS_1 modes. Both the spectral method and the bisection method are capable of finding all the modes that can propagate in the plate. For a transverse isotropic plate with wave number ranges from 10^{-5} m^{-1} up to 12000 m^{-1} with a step size of 100 m^{-1}, and frequency ranging from 10 Hz up to 6 MHz with a step size of 50 Hz, the bisection method succeeds in obtaining the dispersion curves in a time of 1340 seconds. While for the same type of material, the same range of wave number and the number of collocation points of N = 20, the spectral method obtains these curves in 2.816 seconds. This shows the great advantage of using the Spectral method for plotting the dispersion curves with a good convergence and an important time saving.

6.3 Orthotropic material

An orthotropic material has three planes of symmetry orthogonal to each other. It is characterized by nine independent elastic constants. This type of material has been studied by several researchers [20, 27, 39]. The mass density and the elements of the stiffness tensor of this material are reported in Table 7.

Figure 12 shows the dispersion curves plotted by the three methods (DISPERSE, Bisection and Spectral). These curves are superposed on each other. The DISPERSE software presented some ambiguities to plot the dispersion curves. In fact, the Lamb mode S_2 does not appear among the modes presented on Fig. 12a, however, this mode is easily plotted by the two other methods. Moreover, the time taken by the spectral method to obtain these curves in the case of the orthotropic material with the same range of wave number and the number of collocation points mentioned before is 4.540 seconds while the bisection method did it in 1665.4 seconds for the same frequency and wave number ranges presented before.

6.4 Monoclinic material

Now we consider the material used in Section 6.2 with an angle ϕ varying from 0° to 90°. For different values of 0° and 90°, the matrix of elastic constants is similar to that of a monoclinic material.

Table 7. Elastic constants of an orthotropic plate (graphite-epoxy); c'_{ij} (GPa) and ρ (10^3 kg/m^3).

c'_{11}	c'_{12}	c'_{13}	c'_{22}	c'_{23}	c'_{33}	c'_{44}	c'_{55}	c'_{66}	ρ
128	7	6	72	5	32	18	12.25	8	2

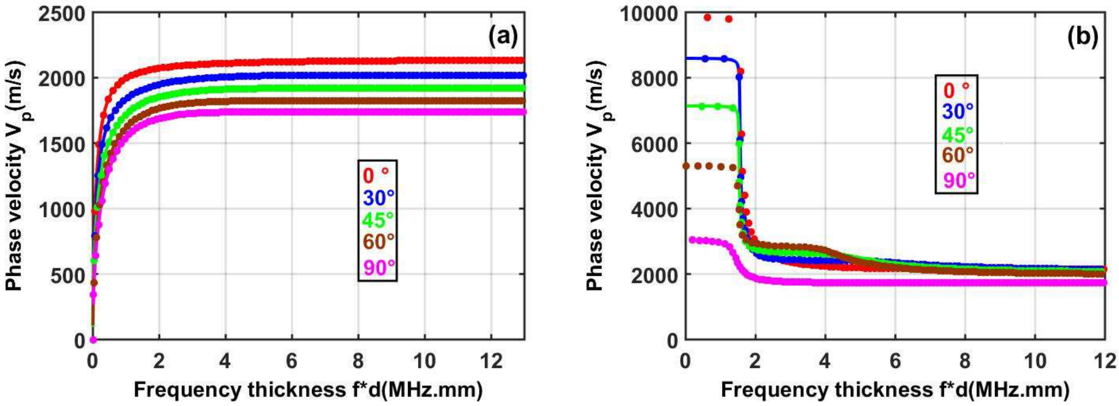

Fig. 13. Influence of the ϕ angle on the first A_0 (a) and S_0 (b) modes, spectral method (•) DISPERSE software (continuous line).

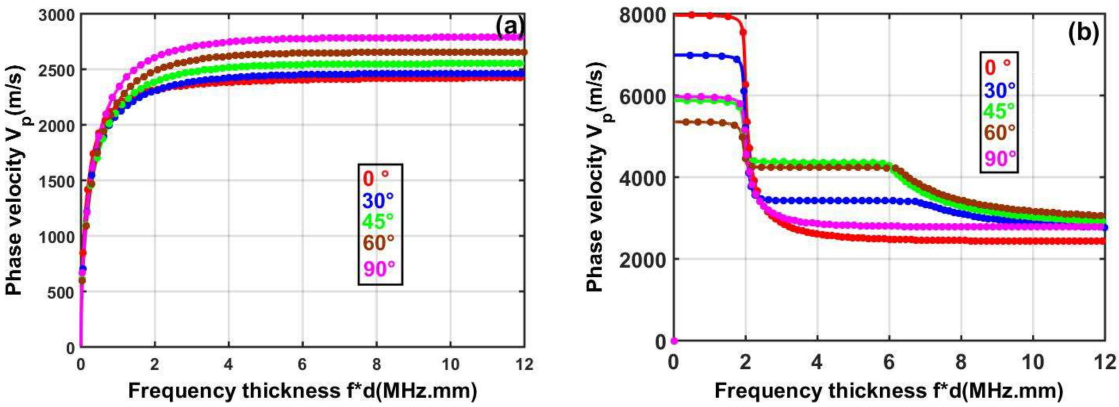

Fig. 14. Influence of the ϕ angle on the first A_0 (a) and S_0 (b) modes, spectral method (•) DISPERSE software (continuous line).

In Fig. 13, we have plotted the phase velocities of the fundamental modes S_0 and A_0 for different values of the ϕ angle (0°, 30°, 45°, 60° and 90°). The spectral method was able to generate easily the dispersion curves of a monoclinic material. These curves are in very good agreement with the results obtained by the DISPERSE software. We notice that there is a dependence between the phase velocity and the ϕ angle. For the A_0 mode, each value of the ϕ angle is characterized by its own phase velocity throughout the frequency range. However, for the S_0 mode (Fig.13b), we observe that we have three regions. At low frequencies f < 500 kHz, for each ϕ angle corresponds to a very distinct phase velocity. Therefore, at the frequency f ≈ 500 kHz, we notice that the phase velocities of the angles 0°, 30°, 45° and 60°, meet in V_P = 4400 m/s. During the control, if we have a doubt about the ϕ angle, this velocity could be exploited to generate the S_0 mode at this frequency.

As a second example, we take the material studied in section 6.3 with the same values of the ϕ angles taken earlier.

In Fig. 14, the phase velocities of the fundamental modes A_0 and S_0 are plotted for the values of the ϕ angle mentioned before. In the same way as the previous example, in the A_0 mode, each value of the ϕ angle corresponds to a proper phase velocity in the whole frequency interval. Regarding the S_0 mode, the phase velocities of the angles 30°, 45° and 90° meets for the couple (f = 500 kHz, V_P = 4550 m/s). We can use this velocity to generate the S_0 mode during a control where we have no information about the ϕ angle.

When the angle has a different value from 0 and 90 degrees, the stiffness matrix has a monoclinic symmetry and this affects the phase velocities of the modes because the Lamb modes are coupled to the SH modes.

7. Comparison with Previous Results

To validate the dispersion curves obtained by the spectral method, we aim in this section to compare our results with those obtained by previous works. Nayfeh [27] illustrated the dispersion curves obtained analytically for different types of materials with various classes of symmetries. In our comparison, we have chosen two types of materials: the first material (Fig. 15a) is the Nickel with cubic symmetry and the second one is an artificial orthotropic material at ϕ = 45° (Fig. 15b).

From Fig. 15 (a and b), we observed that the curves obtained by the spectral method are in very good agreement with those of Nayfeh for both types of symmetries. However, we have been able to dissociate the different families of modes in our curves, moreover, we have succeeded to well define them around the low and high phase velocities.

In order to perform proper non-destructive testing by ultrasonic guided waves, we need the dispersion curves that represent the control frequencies. In addition, we need to know the shape of the generated modes. These profiles allow us to choose the appropriate mode for the control according to the type of defect to detect. In the following, we will present a detailed study of the displacement and stress profiles of the modes that can propagate in a homogeneous and anisotropic elastic planar waveguide.

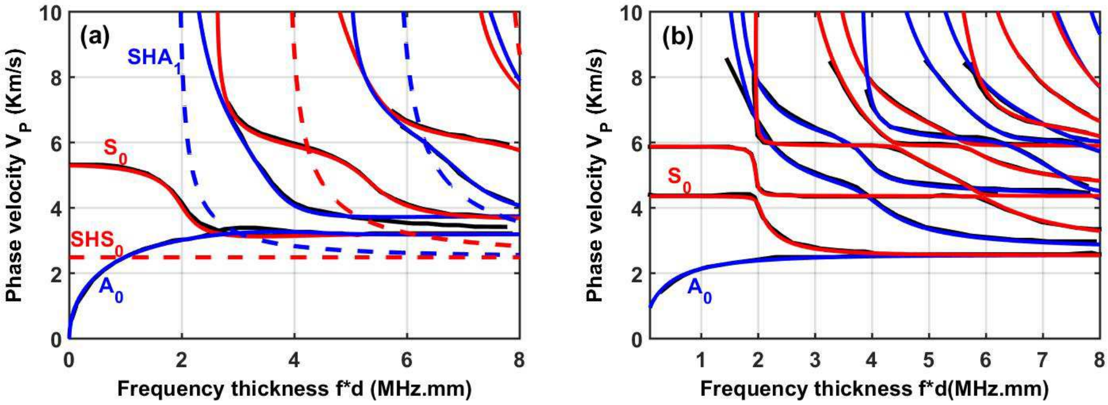

Fig. 15. (a-b) Comparison of the dispersion curves in the (fd, V_P) plane obtained by reference [27] and the spectral method. -Red continuous lines: symmetrical Lamb modes. -Blue continuous lines: antisymmetric Lamb modes. -Red interrupted lines: symmetrical SH modes. -Blue interrupted lines: antisymmetric SH modes. -Black lines: reference solution.

8. Displacement and Stress Field

In this section, we will present a technique for obtaining exact amplitudes of the displacement and stress fields through the thickness of the plate. This technique is based on the normalization of displacement and stress fields by acoustic power [40, 41]. In fact, the profiles of the displacement and stress fields are calculated via the analytical expressions Eq. (10) and Eq. (15) or are deduced from the eigenvectors in the case of the spectral method. The amplitudes of the displacements and stresses are usually calculated analytically as a function of a multiplicative coefficient. While the displacement profiles of the spectral method are provided by the *eig* function of Matlab as normalized eigenvectors in amplitudes, that is, their amplitudes vary between minus one and one. Unfortunately, these amplitudes have no physical meaning. Normalization by acoustic power will provide a solution to this ambiguity.

The normalization of acoustic fields by the acoustic power states that the wave transports a power of 1 Watt through a straight section perpendicular to the direction of propagation of a plate of thickness d = 2h and width 1 meter. This power is calculated by the following expression:

$$P_{ac} = \int_0^1 \int_{-h}^{+h} \vec{P}\vec{n}\, dx_2 dx_3 \tag{26}$$

where $\vec{P}$ is the Poynting vector and $\vec{n}$ is a unit vector parallel to the propagation direction. P_{ac} is a complex number. Its real part will be considered and denoted by P_M :

$$P_M = -\frac{1}{2}\mathrm{Re}\left(\int_{-h}^{+h} (\mathrm{v}^* .\sigma)\vec{\mathrm{n}}\, dx_2\right) \tag{27}$$

with $\mathrm{v} = -i\omega u$ is the velocity vector, v^* its conjugate and σ the stress tensor.

The normalized displacement u_{inor} and stress fields σ_{ijnor} are calculated as follows:

$$\begin{cases} u_{inor} = \dfrac{u_i}{\sqrt{|\,\mathrm{P_M}\,|}} \\ \sigma_{ijnor} = \dfrac{\sigma_{ij}}{\sqrt{|\,\mathrm{P_M}\,|}} \end{cases} \tag{28}$$

in which (i, j)=1, 2, 3.

According to Equation (28), the analytical displacement profiles that depend on a constant are divided by the acoustic power that depends on the same constant. We obtain exact normalized displacement profiles (no more constant). The power normalization will permit to have exact amplitudes of the displacement and stress fields. It will also allow to easily compare the modes susceptible to propagate in a plate and to realize an energy balance during the study, for example, the interaction of a mode by a defect.

Next, we will compare the displacements and stresses normalized in acoustic power to those deduced from the eigenvectors for the spectral method (normalized in power). For this purpose, we consider the orthotropic material defined in section 6.3 with an angle of ϕ = 0°. For this angle, the modes S_n, A_n, SHS_n and SHA_n are generated.

At the frequency f = 500 kHz (the vertical green line marked in Fig. 16), we found the following modes: A_1, S_1, S_0, SHA_1, A_0 and SHS_0 whose wave numbers are, respectively, 306, 351, 511, 1041, 1361 and 1571 m^{-1}.

Figure 17 shows the displacement and stress profiles of symmetric and antisymmetric modes propagating at a frequency of 500 kHz in the orthotropic plate. The verification of the free plate boundary conditions is assured, such that we have the nullity of the stresses σ_{33},σ_{23} and σ_{13} at $x_3 = \pm h$. Lamb modes are characterized by the nullity of the displacement u_2 and the stress σ_{23}. The symmetric character of the S_n modes is observed for displacement u_1 and stress σ_{33}. Antisymmetric behavior is observed for displacement u_3 and stress σ_{13}. The antisymmetric modes A_n present an opposite vibrational behavior.

The horizontal shear modes, polarized in x_2, have a null profile for the displacements u_1 and u_3 as well as for the stresses σ_{33} and σ_{13}. As for the displacement u_2 and the stress σ_{23} they depend on the nature of the mode (SHS_n or SHA_n).

The displacement and stress profiles obtained by the spectral method are in very good agreement with those obtained analytically.

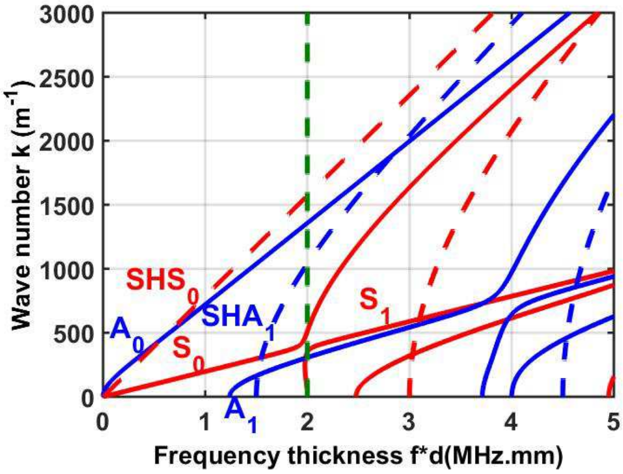

Fig. 16. Dispersion curves in the (fd, k) plane: -Red continuous lines: symmetric Lamb modes. -Blue continuous lines: antisymmetric Lamb modes. -Red interrupted lines: symmetrical SH modes. -Blue interrupted lines: antisymmetric SH modes.

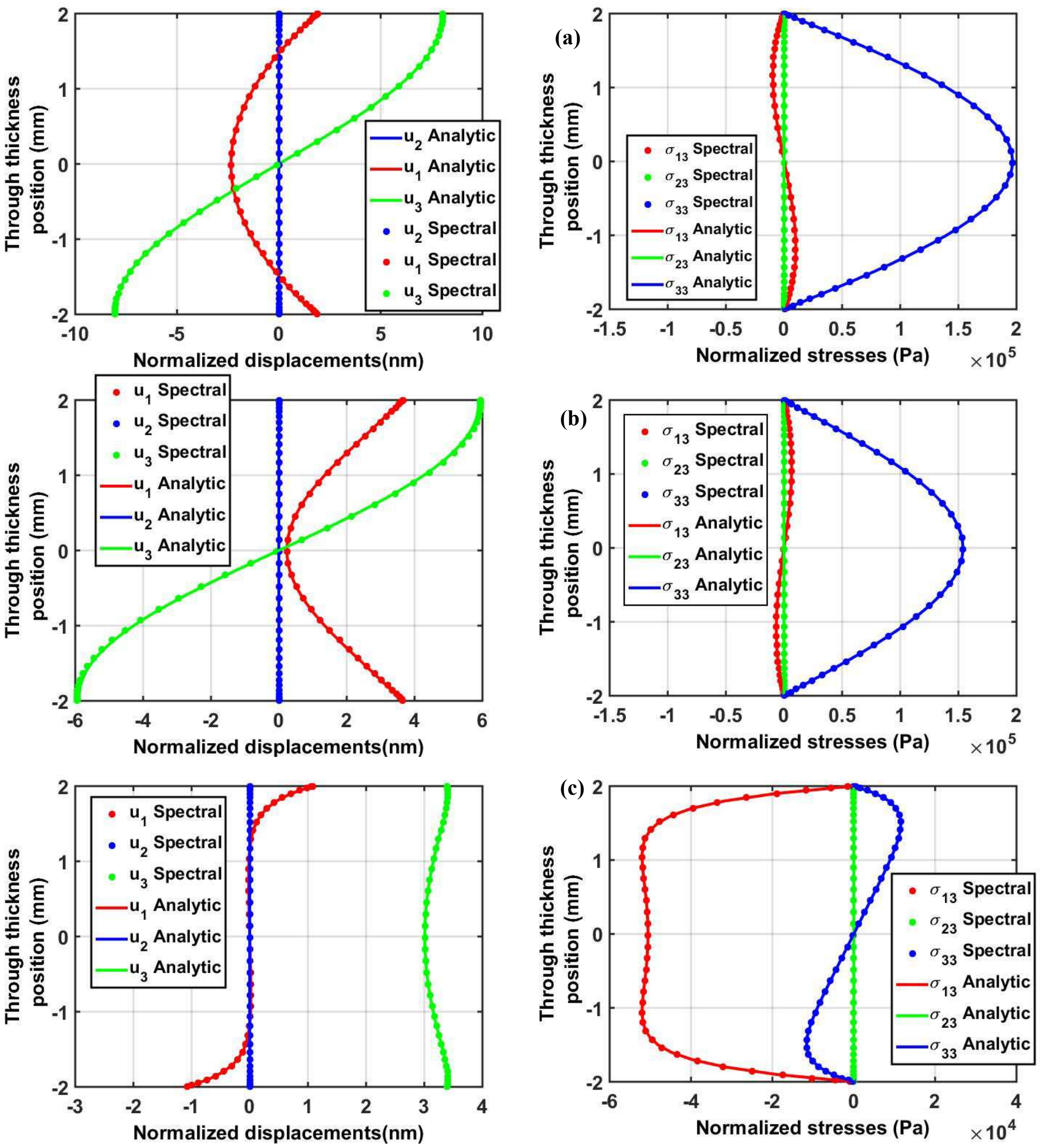

Fig. 17. Normalized displacements and corresponding stresses of the S_0 (a), S_1 (b), A_0 (c), A_1 (d), SHS_0 (e) and SHA_1 (f) modes localized at the frequency f = 500 kHz.

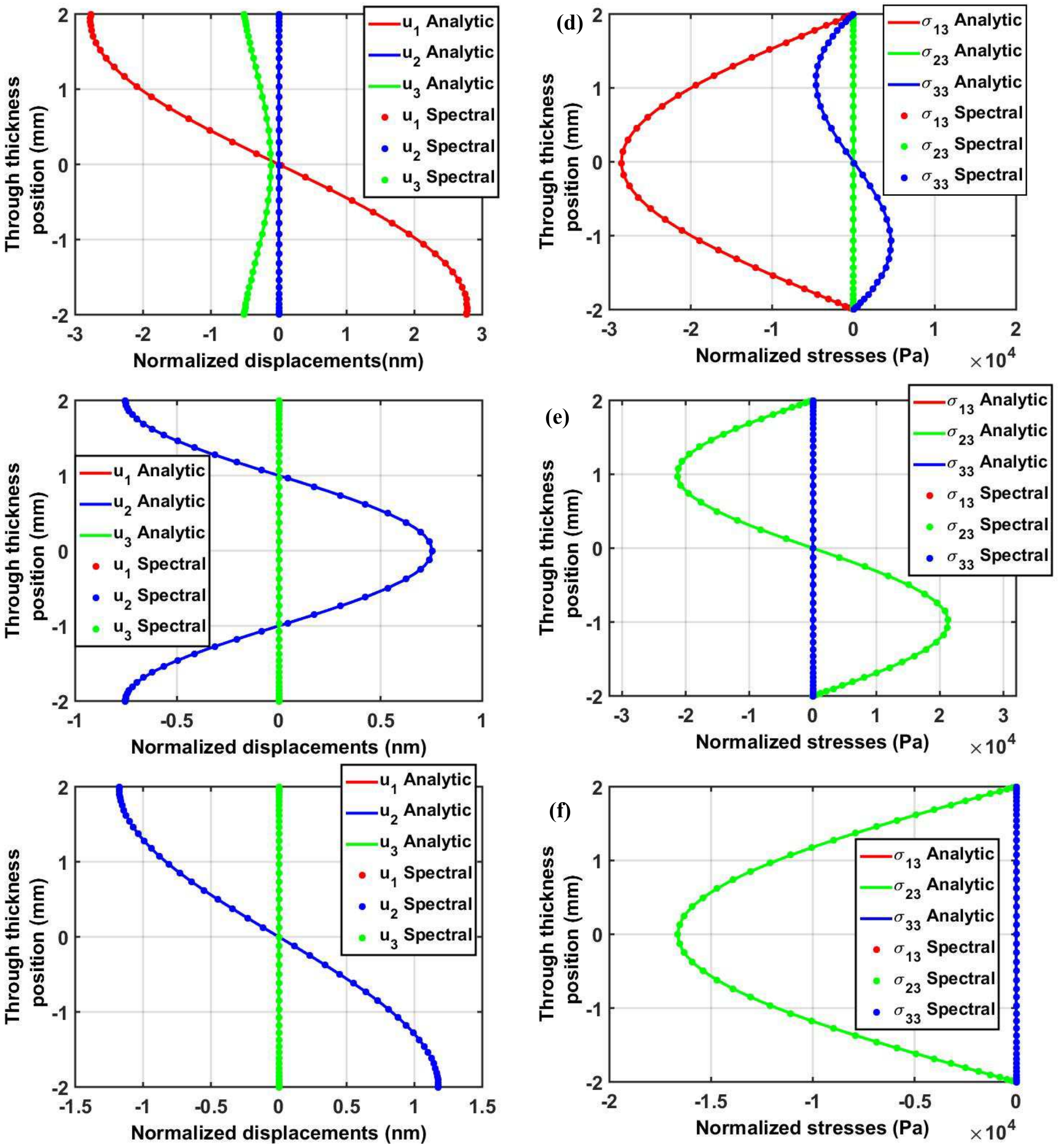

Fig. 17. Continued.

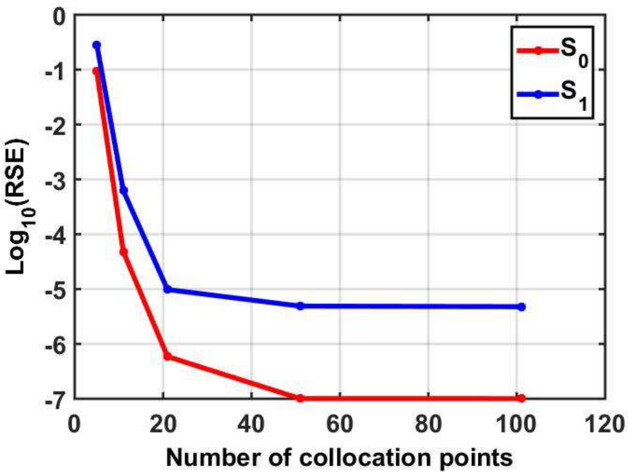

Fig. 18. Decimal logarithm of the RSE for the S_0 and S_1 modes.

Table 8. Root square error for different values of collocation points; RSE=$\sqrt{(u_{1Analytic}-u_{1Spectral})^2}$.

Collocation points	N = 3	N = 5	N = 11	N = 21	N = 51	N = 101
S_0 mode	-	0.0924	4.7952 10^{-5}	5.8723 10^{-7}	1.0067 10^{-7}	1.0056 10^{-7}
S_1 mode	-	0.28591	6.1938 10^{-4}	9.7846 10^{-6}	4.8888 10^{-6}	4.7736 10^{-6}

Table 9. Comparison between the different methods used in anisotropic media.

Materials	Control	Bisection	Newton	Hybrid	Spectral
Transverse isotropic	Computing time (s)	1340	967	905.6	2.8160
	Number of iterations	20467	55591	36636	1 for each value of the wave number
Orthotropic	Computing time (s)	1665.4	1197	1126	4.5400
	Number of iterations	20835	56906	37503	1 for each value of the wave number
Monoclinic $\phi = 60^{\circ}$	Computing time (s)	3718	-	2113	7.4186
	Number of iterations	25818	Inf	45637	1 for each value of the wave number

Next, we study the influence of collocation points on the convergence of eigenvectors. To this end, we calculate the root square error between the analytical displacements and the eigenvectors from the SM. We restrict ourselves to the cases of longitudinal displacement u_1 for the first two symmetric Lamb modes S_0 and S_1 at (f = 500 kHz, k = 511 m^{-1}) and (f = 500 kHz, k = 351 m^{-1}) couples.

In Table 8, the RSE for each value of the collocation points (N = 3, 5, 11, 21, 51 and 101) are plotted in both modes. To obtain the RSE reported in the above table, we calculate the analytical displacements by the same coordinates of the collocation points taken in the SM.

Starting from N = 3, the spectral method does not even provide these modes, but for higher values of N, the S_0 and S_1 modes are calculated. The convergence of the spectral method increases with the number of collocation points (Fig. 18). Arriving at a certain value of N (maximum convergence $N \geq 21$ for our case) where the order of the squared error stabilizes (beyond N = 51). Many researchers [13, 17, 20] have plotted the displacements from the spectral method in the case of waveguides. The symmetry criteria are taken into account for the validation. We present here a well-detailed and precise study for the validation of the displacements and stresses obtained from the spectral method for planar waveguides. This study comes as a complement to previous works [17, 20] on the displacement obtained by the spectral method.

9. Discussion

The DISPERSE software is known for its wide use in the field of non-destructive testing by UGW to generate dispersion curves. Actually, in the case of an isotropic plate, we have obtained all the modes that can propagate in the selected frequency and wave number ranges. However, in the case of anisotropic plates, there were restrictions especially in the case of the S_0 mode, the most commonly used mode in industry and by scientists to examine the pieces by UGW. On the other hand, DISPERSE is a very robust software with many options that facilitate its manipulation by the user.

The spectral method as well as the bisection method allowed us to have accurate solutions without any jump of mode in the different cases studied. The spectral method showed its great advantage over the analytical method from the point of view of computational time so that we had a time saving of about 1337 seconds in the case of a transverse isotropic plate and about 1661 seconds for an orthotropic plate with the same convergence and a low computational effort (Table 9). Moreover, the number of collocation points in the SM does not have a great effect on the accuracy of the solution, but rather on the number of the generated modes. For example, for anisotropic media, if we use the number of points N = 5 we have in our possession the first 9 modes, and for N = 10 the program generates the first 24 modes.

The comparison with the results obtained in the literature showed the efficiency and robustness of the SM. This robustness is expressed by the potential to properly define the modes susceptible to propagate in the anisotropic plate in the whole range of the wave number, and also to dissociate them which represents a great advantage. We then applied the acoustic power normalization method to the analytical displacement fields and the eigenvalues of the SM. It allowed us to obtain normalized displacement and stress profiles of the modes susceptible to propagate in a planar waveguide. The comparison of the analytical and spectral results proved the accuracy of the eigenvectors obtained by the SM. Moreover, we were able to validate the displacements obtained from the eigenvalues of the spectral method.

10. Conclusion

In this paper, we were interested in the study of the spectral method for planar waveguides in ultrasonic non-destructive testing. On this basis, we presented a comparative study between different methods of plotting the dispersion curves for various types of materials. The spectral method showed its robustness to represent the dispersive character of the UGW in different types of material symmetry. Moreover, this method has shown a gain in computational time compared to the classical root finding algorithms with very good convergence and a low coding effort. In addition, the comparison with the results obtained by Nayfeh [27] in the field of non-destructive testing by UGW was made. Very good agreement between the results was noticed. Using the mode separation technique presented in the article, the mode crossing phenomenon is no longer detected. The theoretical approach allowed the knowledge of displacements and stresses according to a constant. As for the spectral method, the displacements from the eigenvectors were normalized in amplitudes, they varied between minus one and one. Due to these incoherencies, the two approaches do not allow us to establish an energy balance on the controlled structure, and therefore the inability to detect the present defects. The normalization by the acoustic power of these fields allowed us to overcome these limits. A comparison between the analytical and spectral displacement and stress profiles has been realized. A very good agreement was observed between them. The study of the convergence order of these profiles as a function of the number of collocation points was essential to determine the optimal distribution of these points. The comparison of the analytical and spectral results proved the accuracy of the eigenvectors obtained by the SM, and comes as a complement to the previous work done by the spectral method [16-21]. As a perspective in our future work, we will establish comparisons between several numerical methods for obtaining dispersion curves (SM, SAFE, Legendre polynomial method, ...) for waveguides of different geometries (plate, cylinder and multilayered system) and character (elastic and viscoelastic) in order to specify the most adequate method to be used with the least coding and computation effort.

Author Contributions

Z. ISMAINE and R. HASSAN planned the scheme of the project. Data collection, formulation, programming and analysis were performed by Z. ISMAINE, R. HASSAN. R. HASSAN and C. ABDELKERIM examined the theory validation. The first draft of the manuscript was written by Z. ISMAINE and all authors commented on previous versions of the manuscript. All authors discussed the results, reviewed, and approved the final version of the manuscript.

Acknowledgments

The authors would like to thank Mr. HONGLEI CHEN for providing us the dispersion curves by the DISPERSE software.

Conflict of Interest

On behalf of all the authors, the corresponding author declares that there is no conflict of interest in the research, authorship, and publication of this paper.

Funding

The authors received no financial support for the research, authorship, and publication of this article.

Data Availability Statements

Not applicable.

References

[1] Stazizar, A.J., Investigation of Flow Phenomena in a transonic Fan Rotor Using Laser Anemometry, *ASME Journal of Engineering for Gas Turbines and Power*, 107(2), 1985, 427-435.
[1] Moser, F., Jacobs, L.J., Qu, J., Modeling elastic wave propagation in waveguides with the finite element method, *NDT & E International*, 32(4), 1999, 225–234.
[2] Valle, C., Niethammer, M., Qu, J., Jacobs, L.J., Crack characterization using guided circumferential waves, *The Journal of the Acoustical Society of America*, 110(3), 2001, 1282–1290.
[3] Li, Y., Thompson, B.R., Influence of anisotropy on the dispersion characteristics of guided ultrasonic plate modes, *The Journal of the Acoustical Society of America*, 87(5), 1990, 1911–1931.
[4] Dayal, V., Kinra, V.K., Leaky lamb waves in an anisotropic plate. I: An exact solution and experiments, *The Journal of the Acoustical Society of America*, 85(6), 1989, 2268–2276.
[5] Ciampa, F., Meo, M., Acoustic emission source localization and velocity determination of the fundamental mode A0 using wavelet analysis and a Newton-based optimization technique, *Smart Materials and Structures*, 19(4), 2010, 045027.
[6] Ndiaye, E.B., Duflo, H., Non-destructive testing of sandwich composites: adhesion defects evaluation; experimental and finite element method simulation comparison, In *Acoustics*, 2012.
[7] Guo, S., Rebillat, M., Mechbal, N., Dichotomy property of dispersion equation of guided waves propagating in anisotropic composite plates, *Mechanical Systems and Signal Processing*, 164, 2022, 108212.
[8] Schwab, F., Knopoff, L., Surface-wave dispersion computations, *Bulletin of the Seismological Society of America*, 60(2), 1970, 321–344.
[9] Mal, A.K., Guided waves in layered solids with interface zones, *International Journal of Engineering Science*, 26(8), 1988, 873–881.
[10] Honarvar, F., Enjilela, E., Sinclair, A.N., An alternative method for plotting dispersion curves, *Ultrasonics*, 49(1), 2009, 15–18.
[11] Waas, G., Earth vibration effects and abatement for military facilities: report 3: analysis method for footing vibrations through layered media, *Waterways Experiment Station*, 1972.
[12] Ahmad, Z., Vivar-Perez, J.M., Gabbert, U., Semi-analytical finite element method for modeling of lamb wave propagation, *CEAS Aeronautical Journal*, 4(1), 2013, 21–33.
[13] Nissabouri, S., Allami, M.E., Boutyour, E.H., Quantitative evaluation of semi-analytical finite element method for modeling lamb waves in orthotropic plates, *Comptes Rendus Mécanique*, 348(5), 2020, 335–350.
[14] Barazanchy, D., Giurgiutiu, V., A comparative convergence and accuracy study of composite guided-ultrasonic wave solution methods: Comparing the unified analytic method, safe method and disperse, *Proceedings of the Institution of Mechanical Engineers, Part C: Journal of Mechanical Engineering Science*, 231(16), 2017, 2961–2973.
[15] Pavlakovic, B., Lowe, M., Alleyne, D., Cawley, P., *Disperse: A general purpose program for creating dispersion curves*, In Review of progress in quantitative nondestructive evaluation, Springer, 1997.
[16] Adamou, A., Craster, R.V., Spectral methods for modelling guided waves in elastic media, *The Journal of the Acoustical Society of America*, 116(3), 2004, 1524-1535.
[17] Karpfinger, F., Gurevich, B., Bakulin, A., Modeling of wave dispersion along cylindrical structures using the spectral method, *The Journal of the Acoustical Society of America*, 124(2), 2008, 859–865.
[18] Karpfinger, F., Valero, H.P., Gurevich, B., Bakulin, A., Sinha, B., Spectral-method algorithm for modeling dispersion of acoustic modes in elastic cylindrical structures, *Geophysics*, 75(3), 2010, 19–27.
[19] Yu, B., Yang, S., Gan, C., Lei, H., A new procedure for exploring the dispersion characteristics of longitudinal guided waves in a multilayered tube with a weak interface, *Journal of Nondestructive Evaluation*, 32(3), 2013, 263–276.
[20] Quintanilla, F.H., Lowe, M.J.S., Craster, R.V., Modeling guided elastic waves in generally anisotropic media using a spectral collocation method, *The Journal of the Acoustical Society of America*, 137(3), 2015, 1180-1194.
[21] Quintanilla, F.H., Lowe, M.J.S., Craster, R.V., Full 3D dispersion curve solutions for guided waves in generally anisotropic media, *Journal of Sound and Vibration*, 363, 2016, 545-559.
[22] Quintanilla, F.H., Lowe, M.J.S., Craster, R.V., The symmetry and coupling properties of solutions in general anisotropic multilayer waveguides, *The Journal of the Acoustical Society of America*, 141(1), 2017, 406-418.
[23] Yu, J.G., Lefebvre, J.E., Guided waves in multilayered hollow cylinders: the improved Legendre polynomial method, *Composite Structures*, 95, 2013, 419-429.
[24] Othmani, C., Dahmen, S., Njeh, A., Ghozlen, M.H.B., Investigation of guided waves propagation in orthotropic viscoelastic carbon–epoxy plate by Legendre polynomial method, *Mechanics Research Communications*, 74, 2016, 27-33.
[25] Zheng, M., He, C., Lu, Y., Wu, B., State-vector formalism and the Legendre polynomial solution for modelling guided waves in anisotropic plates, *Journal of Sound and Vibration*, 412, 2018, 372-388.
[26] Kuznetsov, S.V., Similarity and discrepancy of Lamb wave propagation in functionally graded, stratified, and homogeneous media, *International Journal of Dynamics and Control*, 8(3), 2020, 717-722.
[27] Nayfeh, A.H., Chimenti, D.E., Free wave propagation in plates of general anisotropic media, *Journal of Applied Mechanics*, 56(4), 1989, 881-886.
[28] Eiger, A., Sikorski, K., Stenger, F., A bisection method for systems of nonlinear equations, *ACM Transactions on Mathematical Software*, 10(4), 1984, 367–377.
[29] Kelley, C.T., *Solving nonlinear equations with Newton's method*, SIAM, 2003.

[30] Weideman, J.A., Reddy, S.C., A MATLAB differentiation matrix suite, *ACM Transactions on Mathematical Software*, 26(4), 2000, 465-519.
[31] Huber, A.M., Sause, M.G., Classification of solutions for guided waves in anisotropic composites with large numbers of layers, *The Journal of the Acoustical Society of America*, 144(6), 2018, 3236-3251.
[32] Sanderson, R., A closed form solution method for rapid calculation of guided wave dispersion curves for pipes, *Wave Motion*, 53, 2015, 40–50.
[33] Draudviliene, R., Raišutis, R., Žukauskas, E., Jankauskas, A., Validation of dispersion curve reconstruction techniques for the a0 and s0 modes of lamb waves, *International Journal of Structural Stability and Dynamics*, 14(07), 2014, 1450024.
[34] Crespo, B.H., Courtney, C.R.P., Engineer, B., Calculation of guided wave dispersion characteristics using a three-transducer measurement system, *Applied Sciences*, 8(8), 2018, 1253.
[35] Hernandez-Crespo, B., Engineer, B., Courtney, C., *Empirical technique for dispersion curve creation for guided wave applications*, In 8th European Workshop On Structural Health Monitoring, 2016.
[36] Pant, S., Laliberte, J., Martinez, M., Rocha, B., Derivation and experimental validation of Lamb wave equations for an n-layered anisotropic composite laminate, *Composite Structures*, 111, 2014, 566-579.
[37] Guo, S., *Contribution to the study of guided waves propagation and attenuation in anisotropic composite laminates made up of viscoelastic composite materials: Application to A380 mounted nacelle parts*, Doctoral dissertation, Ecole Nationale Supérieure d'Arts et Métiers Paris, 2021.
[38] Kausel, E., Malischewsky, P., Barbosa, J., Osculations of spectral lines in a layered medium, *Wave Motion*, 56, 2015, 22-42
[39] Li, Y., Thompson, R.B., Influence of anisotropy on the dispersion characteristics of guided ultrasonic plate modes, *The Journal of the Acoustical Society of America*, 87(5), 1990, 1911-1931.
[40] Royer, D., Dieulesaint, E., *Elastic waves in solids I: Free and guided propagation*, Springer Science & Business Media, 1999.
[41] Auld, B.A., *Acoustic fields and waves in solids*, Krieger Pub. Co., 1973.

ORCID iD

Ismaine Zitouni https://orcid.org/0000-0002-3538-2761
Hassan Rhimini https://orcid.org/0000-0002-5784-9844
Abdelkerim Chouaf https://orcid.org/0000-0003-1765-6762

How to cite this article: Zitouni I., Rhimini H., Chouaf A. Comparative Study of the Spectral Method, DISPERSE and Other Classical Methods for Plotting the Dispersion Curves in Anisotropic Plates, *J. Appl. Comput. Mech.*, 9(4), 2023, 955–973. https://doi.org/10.22055/jacm.2023.42530.3941